

Conformal Reflectarray Metasurface

Maryann Benny Fernandes, Ph.D. student

Electrical and Computer Engineering Department, Duke University, Durham, NC, USA

Abstract—To be able to design using numerical simulations a conformal reflectarray metasurface.

Index Terms—reflectarray, conformal, metasurface

I. INTRODUCTION

Reflectarrays are a type of high gain antennas that have originated based on the design and operation of the parabolic dish and the phased array. It possesses two distinct features: the beam pattern, dependent on the array configuration, and the electronic steering of the beam, which is conditional on the phase shift associated with the design.

In the Parabolic Dish, electromagnetic signals reflect when illuminated by a feed from a distance, usually the horn antenna. Although its design is simple, it is steered mechanically to limited angles, and its overall system occupies large areas and is bulky. In the phased array, as seen in “Fig. 1”, in a 0° azimuth Cartesian plot in MATLAB 9.1, Phased Array System Toolbox 3.3 are two cases of element spacing. When the spacing between elements is greater than λ , apart from the desired beam, additional or undesirable beams with similar signal strengths as the primary beam tend to arise at different angles, called grating lobes. These undesirable signals degrade the antenna’s performance, decrease directivity, and create noise that can detect unwanted signals and targets. When the spacing between elements is less than λ , there is no grating lobe, but side lobes stay present with deficient gain, smaller in magnitude than the main beam, making it almost redundant. However, these side lobes can still cause disturbances in systems that require nearly no noise, and further need for suppression becomes necessary through external circuitry or by adjusting the phase shift of the elements accordingly. [1]

Generally, a single isotropic antenna radiates sine waves in all directions. Still, with the addition of another antenna spaced at $\lambda/2$, there is perfect aligning of the phases in the desired direction where the signals constructively interfere and destructively interfere in the remaining regions due to phase mismatch, causing a reduction in the beamwidth of the signal and a slightly higher gain. As visualized in “Fig. 2”, as the number of elements in a phased array increases, the antenna’s gain increases, and beamwidth decreases at the zenith with gain-weak side lobes. But, as the array is beam-steered to 25° Elevation (θ) and 0° Azimuth (ϕ), the primary beam shifts to the steered beam angle and broadens because each element in the array has a different phase shift from its neighboring element. Thus, the array design creates the beam pattern,

and the phase distribution across the array steers the beam. When a phased array is part of a transmitter system, the RF source sends signals to a power distribution network, and each antenna element is given equal power through power splitters. The phase shifting controller connected to each antenna provides an electronic beam steering. This entire process enables the steering of the beam to any desired direction and, while in operation, can simultaneously also establish maintenance of single or multiple elements during failures by not disrupting the phased array antennas functionality to still produce a quality beam as compared to the single reflector, which can halt operation in cases of failure or mechanical maintenance’s. However, this design could be more complex, lossy, and expensive. [2].

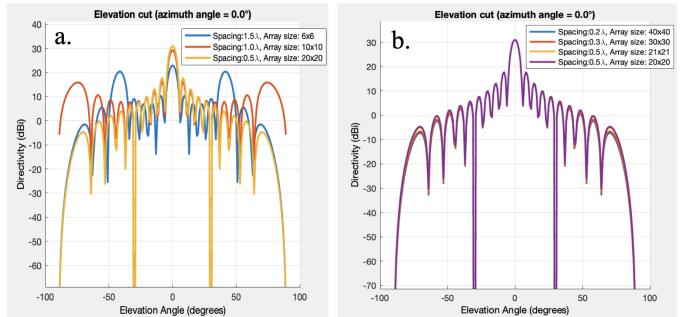


Fig. 1. Equal element spacing in a 300 mm phased array. (a) When spacing is $\geq \lambda$ and (b) $\leq \lambda$.

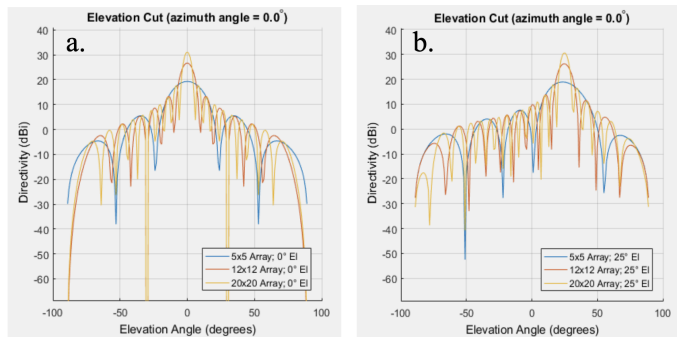


Fig. 2. The array creates the beam pattern and the phase shift steers the beam. (a) Expanding phased array size for three cases without beam steering with equally spaced elements at $\lambda/2$. (b) Expanding array sizes beam-steered at 25° Elevation and 0° Azimuth.

The reflectarray is a reflector that reflects electromagnetic signals when illuminated by a feed from a distance. Its planar structure, based on need can be made conformal and parabolic.

The modulation technique of patch distribution can be either the grayscale patch response where the phase is continuously tuned, or the binary patch response where selective patches are switched on/off via shorting [3]. This architectural design incorporates a compact and lightweight structure for the reflectarray with not-so-complicated fabrications. It can also feature a broad bandwidth through dual [4] or mult-beam [5] patterns from the stacking of multiple layers when illuminated by a single feed. As seen in the Ka-band CubeSat, Integrated Solar Array, and Reflectarray Antenna (ISARA), it can share its aperture with a solar panel on its back [6]. The generation of the reflectarray first originated from the waveguide reflectarray, followed by the spiral phase reflectarray and the microstrip reflectarray. In current times, the technology has evolved to achieve an inflatable and innovative design [7].

II. REFLECTARRAY DESIGN

Reflectarray designs comprise two stages: the system design and the element design. As seen in "Fig. 3", the system design includes the reflectarray and the horn antenna at a far-field distance. The focal length determines the distance to produce a focused beam in the desired direction. The element design is a unit cell tuned to various patch sizes to produce corresponding phase shifts for every variation in size, the grayscale patch response.

A. System design

The reflectarray operates on the principle that the centered-positioned waveguide illuminates plane waves into the flared taper of the horn antenna and illuminates spherical waves at a particular angle to all the regions of the aperture plane. The different angles correspond to a spatial time delay that begins from the center of the aperture and progresses linearly to the edges. Equation 1 is the conventional array equation, where d is the element spacing, λ_o is the wavelength, and θ is the primary beam angle. Considering a broadside (0°) beam angle, the elements in the center are spaced 0.95λ , and progressing towards the edges is made below 0.6λ when the f/D ratio is 0.5 beyond the regions where the incident angle is 45° . This action helps support the idea that if the spacing is large, a primary beam will arise at the broadside, and no grating lobes will appear in the other regions due to the decreased spacing. However, this spacing variation is difficult to manufacture, and equal spacing of elements is considered. In the 300x300 mm reflectarray design, with an array size of 21x21, the elements are spaced at 0.47λ from each other. [1]

$$\frac{d}{\lambda_o} \leq \frac{1}{1 + \sin(\theta)} \quad (1)$$

Equation 2 calculates the spatial time delay, where R_i is the distance from the feed phase center to the i_{th} element, and can be calculated by using either the 3D-Euclidean distance by calculating the distance between the feed and the i_{th} patches center or through Pythagoras theorem, resulting in the same distance value. The feed phase center is the center point of the waveguide terminating end before it enters the

flared region of the horn antenna. k_o is the wavenumber at the center frequency. The spatial time delay is balanced by assigning a phase shift in variable patch sizes. The patches at the center of the aperture are allowed with more delay corresponding to when the illuminated signal reaches the far edges of the aperture. The beam-steered reflected waves radiate simultaneously by providing a phase distribution and the element's size at each location on the aperture, producing plane waves [8].

$$\Phi_{spd} = -k_o R_i \quad (2)$$

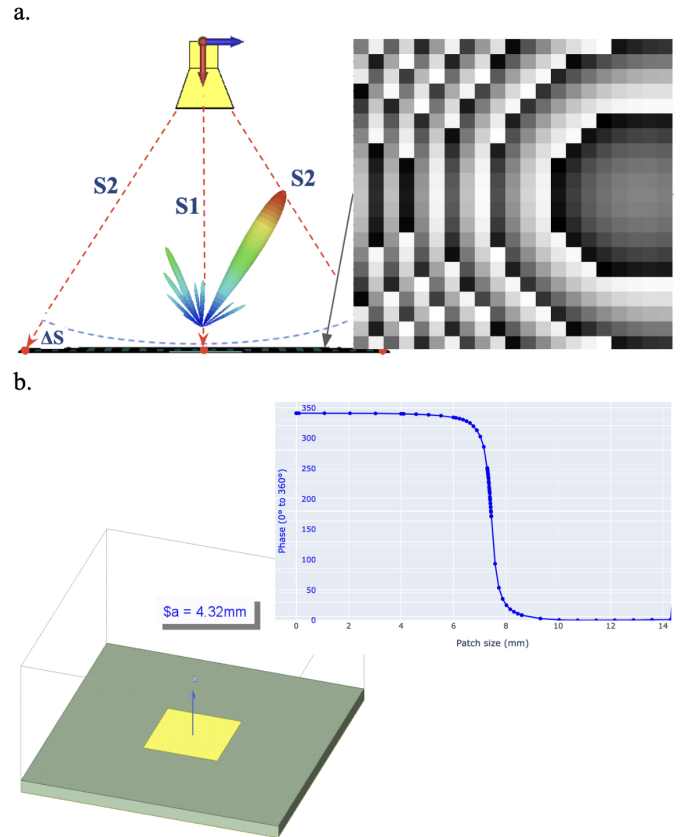


Fig. 3. Reflectarray design workflow. (a) The system design comprises a feed horn illuminating the grayscale patch response reflectarray for beam-steering. (b) The element design is a unit cell tuned from 0 mm to 15 mm, producing a phase shift from 0° to 360° for every variation in size.

The reflectarray operates at 10 GHz at a λ of 30 mm in the 8-12 GHz, X-band range of the electromagnetic spectrum. Its architecture comprises a ground plane, stacked below a dielectric substrate - Rogers R04350B, with a 3.48 dielectric constant (ϵ_r) and a height (h) of 0.762 mm. Above the dielectric substrate is an array of reflecting patch elements. The sandwiched dielectric medium between the ground and the patches is a critical component in reflectarrays. Its thickness and ϵ_r significantly influence the reflectarray's radiation performance. The dielectric material for the ground and the patch elements is copper, an excellent electric conductor that reflects the incident signals on the patches and the ground

plane upward. In an ideal case of a perfect electric conductor (pec), the plane waves, when incident at normal incidence, reflect with a 180° phase shift, 100% of the incident signal at a reflection angle of 0° due to pec's infinity conductivity ($\sigma = \infty$). But, in copper, due to its finite conductivity of 6.1×10^7 S/m, some incident signals are absorbed within its 0.0035 mm thickness material. Using Equation 3, where ω is the angular frequency, μ is the magnetic permeability, and σ is copper's electrical conductivity, the skin depth of copper is $0.66 \mu\text{m}$, almost negligible at microwave frequencies, and so, the phase shift of the reflected signal will be a little off and not exact 180° .

$$\sigma = \sqrt{\frac{2}{\omega \mu \sigma}} \quad (3)$$

1) Horn Antenna: The standard gain-pyramidal horn antenna is one of the simplest and most widely used feed antennae for reflectarrays, phased arrays, and parabolic reflectors. By projecting the inner conductor of a coaxial cable into the waveguide, a quarter-wave monopole antenna sources electromagnetic signals into the hollow rectangular waveguide and transmits them out through the flare and out of the wide taper of the horn into a narrow beam. The length of the flare depends on the impedance matching of the wave impedance of the waveguide with the 377Ω impedance of free space. The flare reduces the reflection of signals back into the waveguide, eliminating standing wave signals due to abrupt impedance changes, edge diffraction, poor signal transmission, reduced directivity, and a wide far-field beam pattern. As seen in "Fig. 4", the horn is flared in both the E-plane (along the b_1 direction) and the H-plane (along the a_1 direction), resulting in its radiation pattern being a combination of both the E-plane and the H-plane sectoral horns, which are two types of horn antennas that radiate through a flare in only one-plane, giving the horns their names [9], [10]. The horn gain at 10 GHz was designed using Computer Simulation Software (CST) and was 13 dBi. The horn was excited at the input port of the 22.86 mm x 10.16 mm, 20 mm long WR90 rectangular waveguide. The flare length from the waveguide output to the 47 mm x 37 mm wide horn taper is 30 mm.

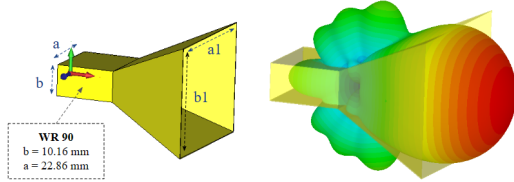


Fig. 4. (a) Standard gain - Pyramidal Horn Antenna a combination of the E-plane and H-plane sectoral horns at 10 GHz. (b) The 3D radiation pattern of the horn simulated with a Directivity of 13 dBi on CST.

The horn antenna is usually set at an offset angle to eliminate the shadow effect caused by a center-fed horn. The horn antenna position, as seen in "Fig. 5" must neither

illuminate a specific portion that causes illumination losses or more than what is required on the aperture plane to produce illumination loss, corresponding to which efficiency of the aperture is realized [11]. When the horn is too close, the gain is high, but the efficiency of the aperture is poor, and high-side lobes emerge due to edge diffraction. When the horn is too far, and when the waves reflect, constructive and destructive interferences occur at the edges of the reflectarray due to edge diffraction, causing poor gain, a broad beamwidth, and high side lobes. The f/D ratio must yield a high directivity, narrow beamwidth, and efficient usage of the reflectarray [1]. The higher the ratio, the narrower the beamwidth; the lower the ratio, the broader the beamwidth. The horn's position is 210 mm from the reflectarray, and the angle from the phase center to the center location of the aperture to its edges is 35.37° , calculated from $\tan(\theta)$ divided by opposite to the adjacent section of the system design.

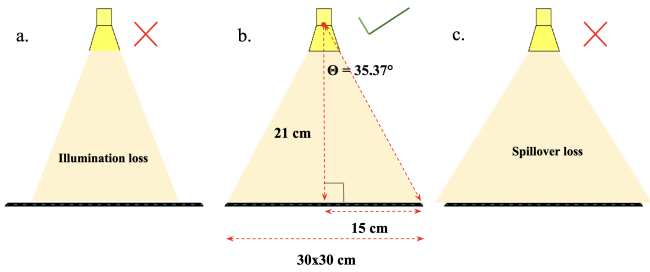


Fig. 5. Illumination of horn on reflectarray. (a) Illumination loss occurs when only a certain portion of the horn is illuminated. (b) To enable efficient use of the reflectarray's aperture the distance of the reflectarray from the horns phase center must be 210 mm and $35.37^\circ \theta$. (c) Illumination loss occurs when the horn illuminates more than the required region of the aperture plane.

2) Phase Distribution: The phase distribution of the reflectarray produces a collimated beam in the desired direction. Equation 4 is the progressive phase distribution without the spatial phase delay. Where k_o is the wavenumber, \hat{r}_i expressed in Equation 5 is the center location of the individual patch element on the aperture, and \hat{r}_o expressed in Equation 6 is the spherical coordinates, are the dot product of each other. (θ, ϕ) is the desired beam direction and (x_i, y_i) is the center location of the i_{th} patch element on the aperture. In Equations 7 and 8, the phase shift assigned to individual elements can be calculated by adding the progressive phase with the spatial phase delay from Equation 1. φ is an additional phase if needed for a particular element. [8], [12]

$$\Phi_{pp} = -k_o \hat{r}_i \cdot \hat{r}_o = -k_o (x_i (\sin \theta \cos \phi) + y_i (\sin \theta \sin \phi)) \quad (4)$$

where,

$$\hat{r}_i = \begin{bmatrix} x_i \\ y_i \end{bmatrix} \quad (5)$$

$$\hat{r}_o = \begin{bmatrix} \sin \theta & \cos \phi \\ \sin \theta & \sin \phi \end{bmatrix} = [\sin \theta \cos \phi, \sin \theta \sin \phi] \quad (6)$$

$$\Phi_{RA} = \varphi_{spd} + \Phi_{pp} \quad (7)$$

$$\Phi_{RA} = k_o(R_i - \sin\theta(x_i \cos\phi + y_i \sin\phi)) + \varphi \quad (8)$$

Using Euclidean distance, as expressed in "Fig. 6", is the distance from the patch to the phase center of the center-fed horn antenna. In "Fig. 7", the phase distribution is calculated using Equation 7. The highest and lowest phase value is 179.63° and -179.41° , providing a 359.04° phase distribution when θ is 30° and ϕ is 0° .

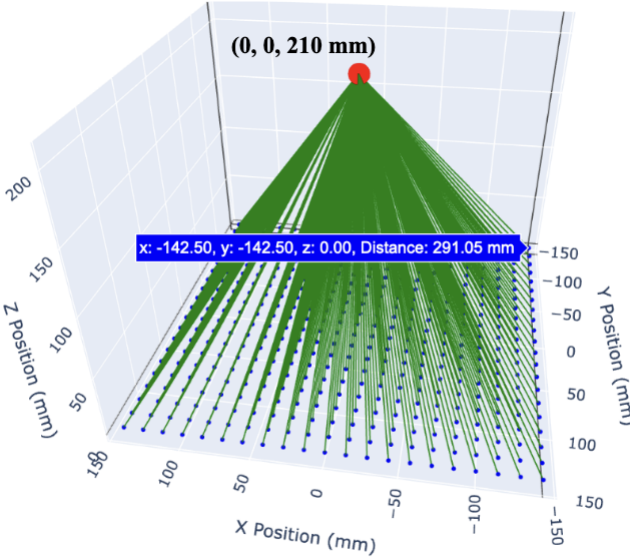


Fig. 6. The distance, R_i , from Equation 1 is obtained by taking the 3D-Euclidean distance of the phase center location and the center location coordinates for all $21 \times 21 = 441$ elements (x_i, y_i). The phase center of the horn is denoted by the red dot.

B. Unit-cell Element design

The unit cell, the element design, is the simplest but also the most important aspect of the reflectarray. It is used to perform interpolation with the data from the phase distribution data to determine the patch size distribution on the reflectarray. Depending on the clarity in the unit cell design, the reflectarray, will produce a directed beam accordingly.

As seen in "Fig. 8", the unit cell comprises a copper-assigned ground plane, the Rogers 4350B dielectric substrate, and the copper-assigned patch element. The boundary conditions are unit cell on the sides, copper ($\text{Et} = 0$) at the bottom and open in the region above the patch. The distance of the plane waves (TEM) excitation from the patch is $\lambda/4$. The mesh box helps to increase the meshing in the patch region for more accurate results of unit cell and has the same dimensions as that of the patch even when tuned to different sizes. In Equation 9 and 10, the uniform sinusoidal varying electric field in the x-direction and the magnetic field in the y-direction, is a function of distance and time along the z-direction, the

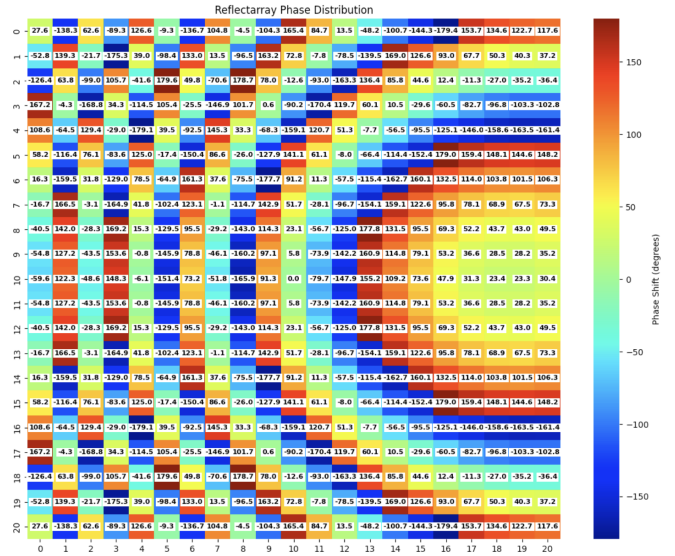


Fig. 7. Phase Distribution of the 300 mm reflectarray with an array size of 21×21 . The numbers on each block and the 180° to -180° colorbar signify the phase shift associated with each element on the array when $\theta = 30^\circ$ and $\phi = 0^\circ$, and the xy axis specifies the element number in a row-column format.

direction of propagation (k). In Equation 11, the electric field is a plane wave and so is its corresponding magnetic field.

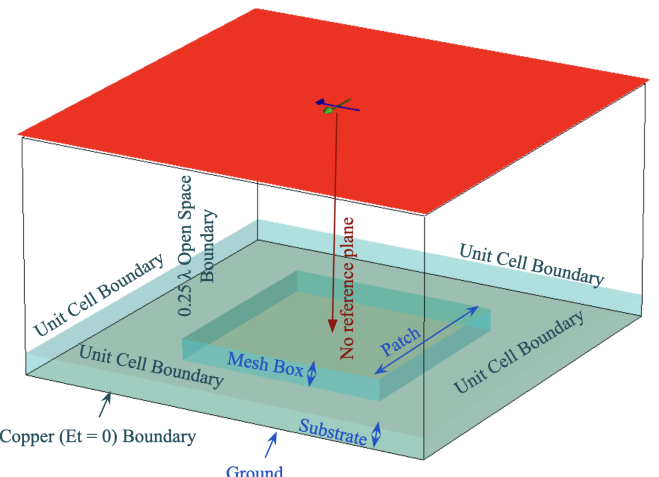


Fig. 8. Unit cell setup on CST

$$\hat{E} = E_o \cos(\beta z - \omega t) \hat{x} \quad (9)$$

$$\hat{H} = H_o \cos(\beta z - \omega t) \hat{y} \quad (10)$$

$$E_x = E_x^+ e^{-j\beta z} + E_x^- e^{j\beta z} \quad (11)$$

$$H_y = \frac{\beta}{\omega\mu} E_x^+ e^{-j\beta z} - \frac{\beta}{\omega\mu} E_x^- e^{j\beta z} \quad (12)$$

"Fig. 9" is the design characteristics of the unit cell. At 10 GHz, the copper square patch ($L=W$) is 7.5 mm ($\lambda/4$) and the criteria is that $W/h \geq 1$ and the thickness of the copper material must satisfy $t \leq \lambda$. The refractive index (η) of the sandwiched dielectric medium determines how waves are slowed down in the medium, using ($\sqrt{\epsilon_r}$), which is around 1.8 for Rogers R04350B. When waves travel from a lower η_1 to a higher η_2 , the waves reflect with a 180° phase shift, and when they flow from a higher η_1 to a lower η_2 , the reflected waves have no phase shift. When selecting the height of the dielectric constant of the medium, the following criteria must be satisfied $0.003\lambda \leq h \leq 0.05\lambda$ and $2.2 \leq \epsilon_r \leq 12$. Due to fringing effects, as seen in Equation 13, the effective dielectric constant (ϵ_{eff}) is considered and must satisfy $1 \leq \epsilon_{eff} \leq \epsilon_r$. Additionally, the fringing effects also causes the length of the patch to be extended and so its length extension must also be considered as seen in Equation 14 and 15. Typically, the bandwidth of a single patch is very narrow around 2-5%, and with the use of a thicker substrates, a wide bandwidth is obtained but with drawbacks, such as the generation of surface waves in the substrate and its ability to coat around the dielectric during excitation, which can degrade radiation by propagating into the substrate and proportionally affecting gain and beamwidth [13], [14].

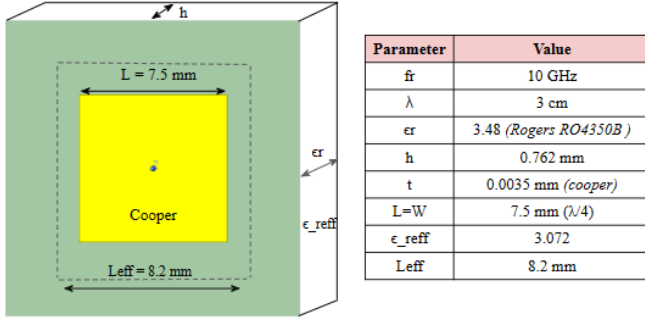


Fig. 9. Unit cell setup on CST

$$\epsilon_{eff} = \frac{\epsilon_r + 1}{2} + \frac{\epsilon_r - 1}{2} \left[1 + 12 \frac{h}{W} \right]^{-1/2} \quad (13)$$

$$\frac{\Delta L}{h} = 0.412 \frac{(\epsilon_{eff} + 0.3) (\frac{W}{h} + 0.264)}{(\epsilon_{eff} - 0.258) (\frac{W}{h} + 0.8)} \quad (14)$$

$$L_{eff} = L + 2\Delta L \quad (15)$$

To obtain the phase shift of the different sizes of patches, as seen in "Fig. 10", a parametric sweep on CST must be performed on the patch. The patch is tuned from 0 - 10.33 mm, and the raw data is obtained. De-embedding, by assigning a reference plane from the port to the patch, produces accurate results for the S-parameters of the patch and its reflection phase, as visualized in "Fig. 11". In this case, there is no mesh box and the unit cell is tuned from 0 - 15 mm. The scattering parameter is very poor and almost all of the data is reflected

from the patch as seen in the reflection coefficient, grey dotted data and the wrapped phase shift from 180° to -180° is denoted by blue and its normalized data from 0° to 360° is denoted in red. Also, it is to be noted that that theoretically, nothing changes in the design of the unit cell and its performance but the accuracy of the data.

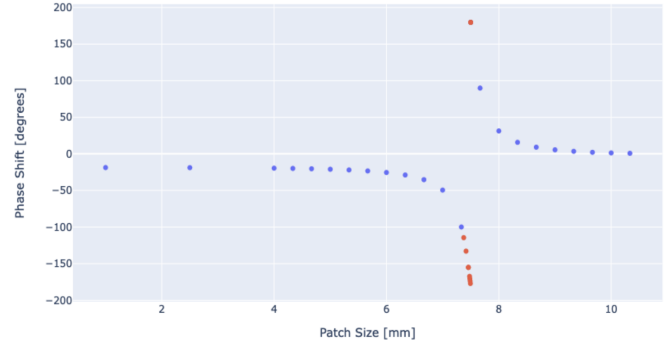


Fig. 10. Patch size versus Phase Shift performed from a parametric sweep on the unit cell on CST. The port to the patch has no reference plane.

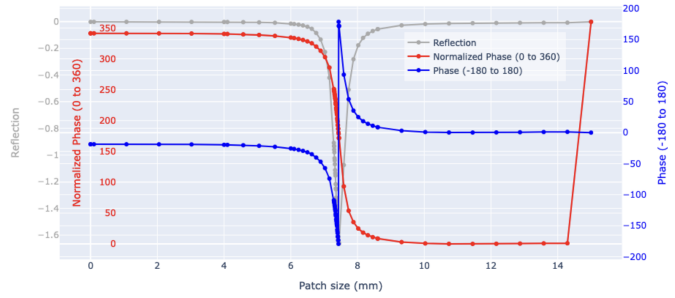


Fig. 11. The port to the patch has a reference plane and is deembeded. The grey dotted line is the reflection coefficient, the blue line is the raw reflection phase data and the red line is the normalized data.

With the data of phase shift of every patch obtained from the phase distribution of the reflectarray, its patch size can now be estimated by performing the linear interpolation with the known data of the unit cell as seen in "Fig. 12". The red line is the CST simulation data from "Fig. 11" and the blue line is the interpolated data. The lowest patch size is 1.62 mm and the highest is 10.24 mm. Accordingly, as seen in "Fig. 13", the patch size distribution values are denoted in the numerical values and its corresponding dimension is denoted by the dotted lines and with the colormap. Additionally, the linear interpolation of the deembeded unit cell with the phase distribution data is as seen in "Fig. 14".

III. PLANAR REFLECTARRAY RESULTS

As seen in "Fig. 15", the planar reflectarray is designed on CST. Using HFSS, the CAD model of the patch array was designed and imported into CST. The design process of the reflectarray design is a horn antenna positioned at the origin of the coordinate system, and excited by a waveguide port at 10 GHz. The distance of the horn from the origin to the

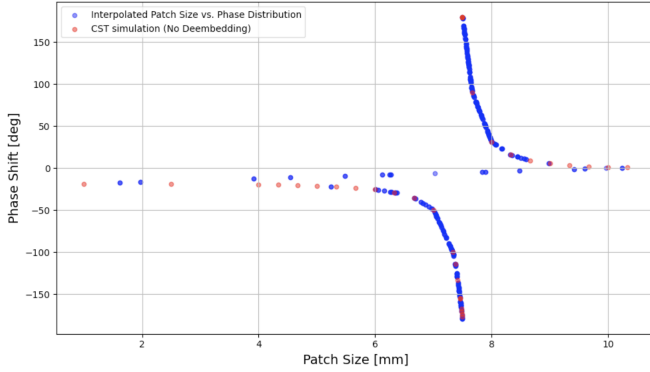


Fig. 12. Linear Interpolation of the known phase shift of the reflectarray from the phase distribution with the known CST data of the patch size versus phase shift.

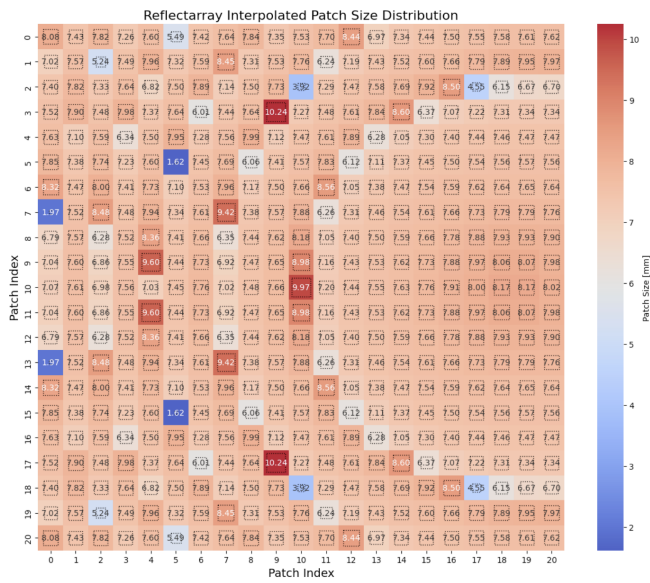


Fig. 13. Patch Size distribution, the numbers denote the value of the patch size and the dotted lines are its corresponding dimension at the location. The colormap is for visualization only and it ranges from 0 - 10.33 mm. The patch index denotes the 21x21 rows and columns in the reflectarray.

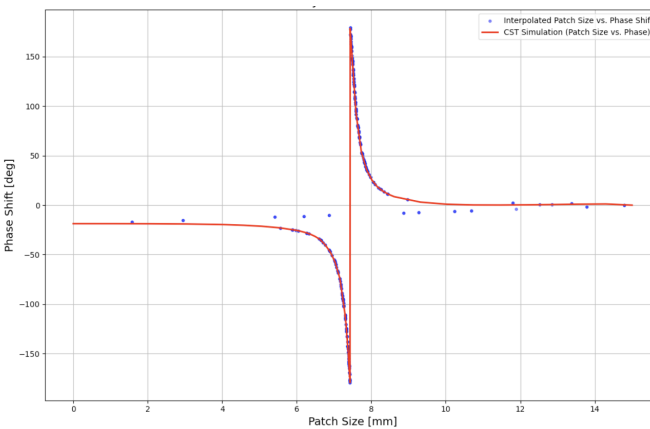


Fig. 14. Linear Interpolation the deembedded unit cell with the phase distribution data

reflectarray is 230 mm, considering the 20 mm height of the waveguide and the 210 mm distance of the phase center to the reflectarray. The patches denoted in yellow are copper, and denoted in green is the 0.762 mm thick substrate and below the substrate is the ground plane. The boundary conditions are kept open on all sides and as seen in "Fig. 16", when the reflectarray is simulated when θ is 0° and ϕ is also 0° , the reflectarray resonates at zenith as visualized by the 3D radiation pattern and the polar plot, where the directivity of the reflectarray is 26.62 dBi and the side-lobe are -11.4 dB. When the reflectarray is beam-steered to $30^\circ \theta$ and $0^\circ \phi$, obtained from the interpolation of the patches in "Fig. 17", the directivity is 24.6 dBi and the side-lobes are -8.8 dB. As seen in "Fig. 18", in-order to suppress the side-lobe, the spacing between all elements is kept at $\lambda/3$, and accordingly, the directivity of the reflectarray increased at 9.5 GHz to 27.32 dBi and the side-lobe were suppressed to -17.2 dB.

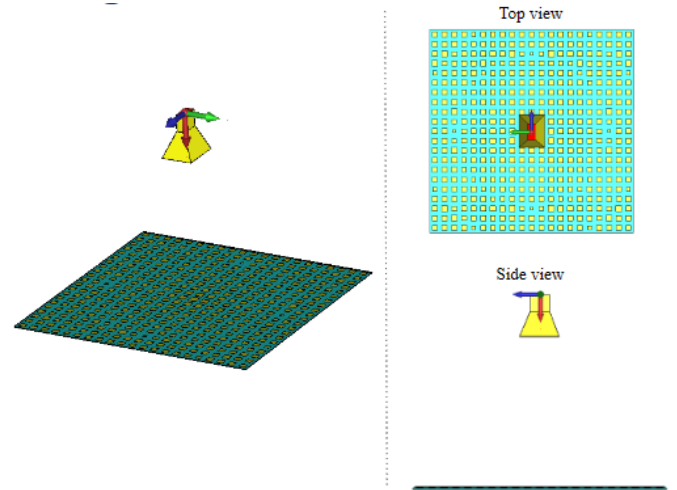


Fig. 15. Planar reflectarray design on CST at 10 GHz

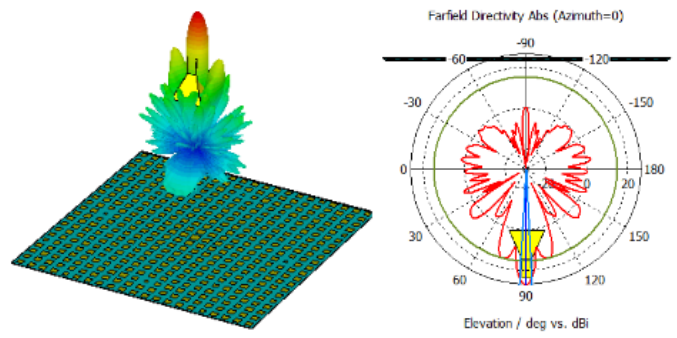


Fig. 16. reflectarray is beam-steered to $0^\circ \theta$ and $0^\circ \phi$, and the directivity is 26.62 dBi and the side-lobe are -11.4 dB.

IV. CONFORMAL REFLECTARRAY RESULTS

As seen in "Fig. 19", the planar reflectarray when θ is 0° and ϕ is also 0° is made conformal for three cases. Case 1 is

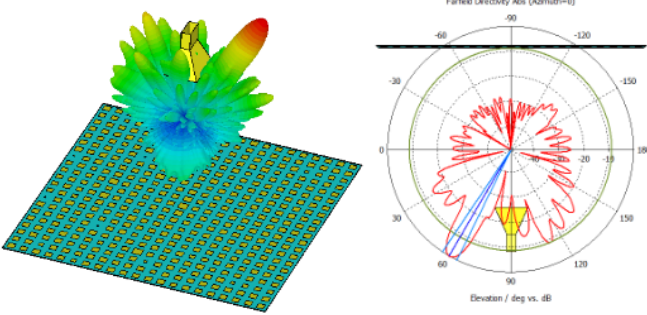


Fig. 17. Reflectarray is beam-steered to $30^\circ \theta$ and $0^\circ \phi$, and the directivity is 24.6 dB and the side-lobes are -8.8.

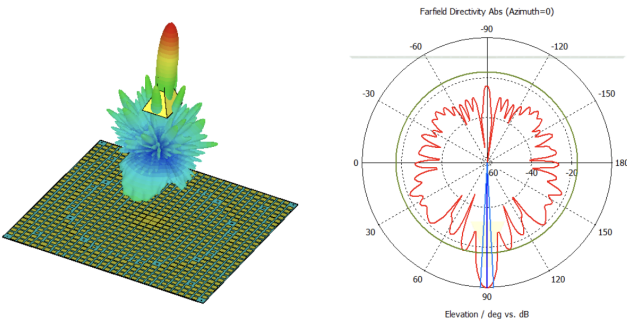


Fig. 18. Reflectarrays with $\lambda/3$ element spacing has a directivity of 27.32 dB and the side-lobes are suppressed to -17.2 dB at 9.5 GHz as seen in its 3D- radiation pattern and polar plot

when the deviation as denoted by the red dots at the center and at the two edges of the reflectarray is $0.012\lambda = 0.36$ mm, obtained by using a cylinder of size $1000\lambda = 30000$ mm. Case 2 is when the deviation as denoted by the red dots at the center and at the two edges of the reflectarray is $0.014\lambda = 4.2$ mm, obtained by using a cylinder of size $87\lambda = 2610$ mm and Case 3 is when the deviation as denoted by the red dots at the center and at the two edges of the reflectarray is $1.62\lambda = 49$ mm, obtained by using a cylinder of size $7\lambda = 210$ mm. These deformation and conformality as seen in 'Fig. 20', degrades the performance of the reflectarray. Without the bent, the original reflectarray design had a directivity of 26.62 dB and as it was made conformal for all three cases, the primary beam is stretched in the direction of the deviation, making the beam broader with respect to its deviation size, degrading the performance of the reflectarrays and it overall directivity strength to 21.97 dB, 19.35 dB and 15.02 dB. The same would occur if the reflectarray were to be steered in a different direction. Additionally, based on the linear interpolation data from 'Fig. 14', the reflectarray when θ is 0° and ϕ is also 0° has a directivity of 26.97 dB as visualized in 'Fig. 21'. To also note that the element spacing between the elements was $\lambda/2.1$ and the distance of the of the reflectarray from the waveguide input was 260 mm. Accordingly when the

reflectarray was made conformal, it degraded with deviations at 0.14λ and 1.71λ to directivity of 19.98 dB and 14.62 dB. When this data was beam-steered, the directivity was 25.8 dB and side lobe was -11.8 dB. This concludes that even with the deembedding and non-deembedding of the unit cell, there was no drastic change in the reflectarrays performance except for the how the unit cell reflection phase data was calculated.

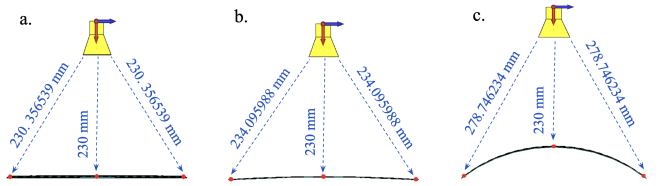


Fig. 19. Deviating and making conformal the planar reflectarray for three cases when radius of the cylinder is 1000λ , 87λ and 7λ and deviations are 0.012λ , 0.14λ and 1.62λ

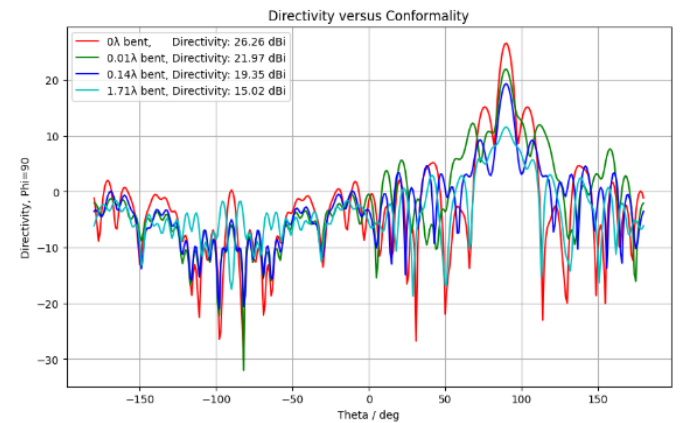


Fig. 20. Directivity versus conformality of the reflectarray, the directivity decreases as the deviation increases when the unit cell was not deembedded.

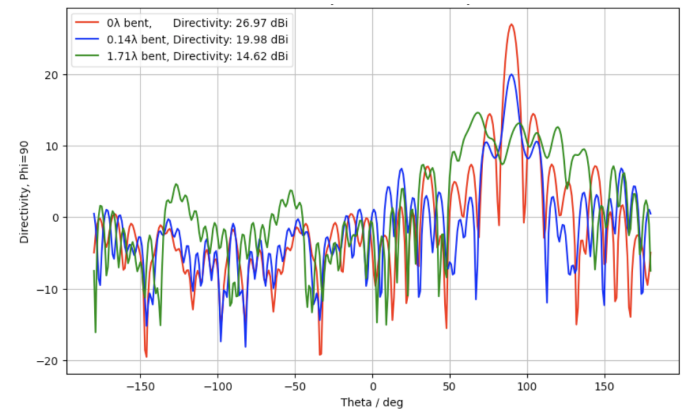


Fig. 21. Directivity versus conformality of the reflectarray when the unit cell was deembedded.

CONCLUSION

The mathematical and numerical simulations of a conformal reflectarray metasurface was confirmed for different three

cases when radius of the cylinder was assigned at 1000λ , 87λ and 7λ and accordingly their deviations were 0.012λ , 0.14λ and 1.62λ .

ACKNOWLEDGMENT

I would like to acknowledge the mentorship and support on this project by my Ph.D. advisor, Distinguished Professor Dr. David R. Smith of Duke University, and my mentor Dr. Divya Pande, Research Associate at Duke University and Research Scientist at Metacept.

REFERENCES

- [1] Huang and Encinar, Reflectarray antennas (2008), Chapter 4.
- [2] V. Jamnejad, J. Huang and R. J. Cesarone, A Study of Phased Array Antennas for NASA's Deep Space Network, Researchgate (2001).
- [3] Aaron V. Diebold, et al., Reflectarray Design Using a Discrete Dipole Framework, IEEE Antennas and Propagation (2023).
- [4] J.A. Encinar, Design of two-layer printed reflectarrays using patches of variable size, IEEE Transactions on Antennas and Propagation, Vol. 47, Issue: 10, October 2001, pp. 1403 – 1410.
- [5] J. A. Encinar and J. A. Zornoza , Broadband design of three - layer printed reflectarrays, IEEE Transactions on Antennas and Propagation, Vol. 51, July 2003, Page(s): 1403 - 1410.
- [6] Richard E. Hodges et al, Novel deployable reflectarray antennas for CubeSat communications, IEEE MTT-S International Microwave Symposium (2015).
- [7] Huang and Encinar, Reflectarray antennas (2008), Chapter 2.
- [8] Huang and Encinar, Reflectarray antennas (2008), Chapter 3.
- [9] Constantine A. Balanis, Antenna Theory Analysis and Design, 3rd Edition, Chapter 13.
- [10] Horn Antenna, Wikipedia
- [11] M. Hashim Dahri et al., Aspects of Efficiency Enhancement in Reflectarrays with Analytical Investigation and Accurate Measurement, MDPI (2020)
- [12] P Nayeri, F Yang and AZ Elsherbeni, Reflectarray antennas: theory, designs, and applications (2018).
- [13] M. Kara, Effects of Substrate Thickness on the Properties of Rectangular Microstrip Antenna Elements, AMPC Asia-Pacific Microwave Conference, IEEE, 11-13 August 1992.
- [14] Constantine A. Balanis, Antenna Theory Analysis and Design, 3rd Edition